To cite this article: WANG W J, WANG G X, LI B, et al. Control system design and experiment for large-scale high-speed unmanned underwater vehicle [J/OL]. Chinese Journal of Ship Research, 2020, 15(2). http://www.ship-research.com/EN/Y2020/V15/I2/95.

DOI: 10.19693/j.issn.1673-3185. 01759

Control system design and experiment for large-scale high-speed unmanned underwater vehicle

*WANG Wenjin, WANG Guanxue, LI Ben, XU Guohua**

School of Naval Architecture and Ocean Engineering, Huazhong University of Science and Technology, Wuhan 430074, China

Abstract: [**Objectives**] In order to guide a large-scale high-speed unmanned underwater vehicle (UUV) along the desired path smoothly in 3D space while taking the task requirements of its control performance and hydrodynamics into consideration, a fuzzy line-of-sight (LOS) guidance law with robustness is proposed. [**Methods**] Based on decoupling control, an integrated separate PID algorithm is designed for velocity, heading, depth and pitch. The dynamic characteristics are then modified by introducing filters for commands and state feedback. Finally, the control performance under varying velocities is tested by conducting lake trials. [**Results**] The experimental results show that, under the velocities of 6, 9, 13 kn, the vehicle can follow the desired path and depth within a reasonable margin of error, which demonstrates that the proposed control system is valid. [**Conclusions**] Besides, the achievements lay a theoretical foundation for the motion control algorithm design of next-generation unmanned underwater test vehicles.

Key words: unmanned underwater vehicle (UUV); test vehicle; adaptive guidance; integrated separate PID; second order filter

CLC number: U675.73

0 Introduction

Unmanned underwater vehicles (UUV) are playing an irreplaceable role in more and more fields. Unmanned underwater test vehicles are special UUVs, which are developed based on the submarine self-propulsion models designed and constructed based on the similarity theory. They can be used for comprehensive tests of navigation performance, such as maneuverability, rapidity, and invisibility. Simulation using unmanned underwater test vehicles can yield reliable and direct data that can be used for mutual verification and complementation with test results of towing tanks and wind-tunnel constraint models. Moreover, most of the test results can be applied to actual submarines and will be extended to unmanned submarines in the future to facilitate their development. Therefore, this is a new technology worth developing [1-3].

As early as the 1950s, the US Navy developed a conventionally-powered high-speed manned test vehicle, "Albacore" submarine, which is considered the predecessor of unmanned underwater test vehicles [4]. Then, in the 1970s - 1990s, based on various performance indexes of three nuclear attack submarines under development, the U.S. Navy developed three unmanned underwater test vehicles in the research and demonstration. This provided technical

Received: 2019 - 09 - 05 **Accepted:** 2020 - 01 - 08

Authors: WANG Wenjin, male, born in 1994, Ph.D. candidate. Research interest: control technology of underwater vehicles. E-mail: d201677414@hust.edu.cn

WANG Guanxue, male, born in 1992, Ph.D. candidate. Research interest: control technology of underwater vehicles. E-mail: 379759609@qq.com

LI Ben, male, born in 1994, Ph.D. candidate. Research interest: control technology of underwater vehicles. E-mail: 1039741910@qq.com

XU Guohua, male, born in 1965, Ph.D., professor. Research interest: the technologies of underwater vehicles, intelligent control, and marine-engine automation. E-mail: hustxu@sina.vip.com

***Corresponding author:** XU Guohua

support for the design of pump-jet propellers of submarines, hydrodynamic layout, and control-surface design of low-noise ships, and verification of many other new technologies and equipment [4-7]. At the beginning of independent development of submarines, China proposed developing unmanned underwater test vehicles. So far, a series of work has been carried out, which mainly focused on research imitation and local improvement. Specifically, Liu et al. [8] have completed conventional verification tests on the maneuverability of test vehicles. Thus, they have accumulated technical experience in multiple aspects, such as manufacturing, underwater communication, real-time trajectory tracking, maneuverability testing, and data processing and analysis.

The large-scale high-speed UUV (hereinafter referred to as unmanned vehicle) studied in this paper is a kind of UUV developed for testing rapidity and invisibility. Meanwhile, it is also a new-generation submarine self-propulsion model in China. This unmanned vehicle includes various complex devices and travels at a high test speed. In addition, it is given strict requirements on the accuracy of pose control during testing. Therefore, it is a challenge to design a control system and a navigation control algorithm for the unmanned vehicle. A typical test condition of this unmanned vehicle is path tracking. However, the test vehicle developed by Naval University of Engineering is of no reference due to its low test speed and its focus on maneuverability testing[8]. For this reason, this paper intends to summarize path-tracking algorithms of autonomous underwater vehicles (AUVs). On the one hand, AUVs cruise at a speed. On the other hand, the path-tracking algorithms adopted by AUVs usually decompose a spatial path-tracking problem into path-tracking problems in horizontal and vertical planes. Although these plane-guidance methods can realize established path tracking, for three-dimensional (3D) curve-path tracking, it is a better choice to directly calculate guidance laws in 3D space. Moreover, the unmanned underwater vehicle studied in this paper needs to be tested in a wide speed range. Therefore, it is required that guidance laws should be speed-adaptive. For this reason, this paper intends to briefly summarize the function and framework of the control system of the unmanned vehicle and explain the working principles of key technologies such as 3D adaptive guidance and motion control. In addition, it will show the performance of the control system of the large-scale high-speed UUV through lake trials and result analysis.

1 Overview of unmanned vehicle

This unmanned vehicle model was made according to a specific submarine on a reduced scale, with a total length of about 11 m, displacement of about 8 t, and a designed maximum speed of 17 kn. As a platform for performance tests of propellers, it employs lithium batteries for power supply to the whole vehicle, and is equipped with new propellers to be tested. In addition, the unmanned vehicle uses sail rudders, steering rudders, and separable stern rudders for attitude adjustment. It also carries a high-precision inertial navigation system, a Doppler velocity log (DVL), a depth meter, an altimeter, and anticollision sonar to provide accurate navigation information. This ensures safe navigation of the unmanned vehicle in limited waters.

Besides, the unmanned vehicle has three working modes: surface wireless remote control, optical-fiber remote control, and underwater autonomous navigation. It can realize multiple maneuvering movements required by test tasks, such as surface direct navigation, surface turning, and fixed-depth direct navigation. Meanwhile, it can measure and record multiple characteristic parameters in maneuvering processes. Fig. 1 shows the basic process of an unmanned-vehicle test.

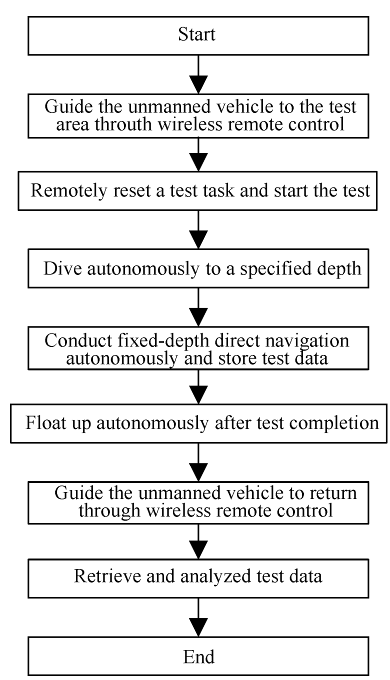

Fig. 1 Basic process of test for the UUV

The unmanned vehicle has greater displacement, and its speed is three to four times that of a conventional AUV. Increased inertia will extend the time of the vehicle to respond rudder operation, and high speed intensifies coupling among degrees of freedom of the vehicle. All of the above increases the difficulty of navigation control.

2 Framework of the control system

The unmanned vehicle carries many devices with different interfacial forms. Thus, such devices need to be managed efficiently to avoid excessive load due to the use of a single controller, and modularization of hardware should be improved for better management. For these purposes, an underwater main control unit, a navigation unit, a motion planning and control unit, a power unit, a basic control unit, an emergency unit, and an underwater data storage unit are designed respectively, according to functional requirements. Specifically, the emergency unit can monitor operational states of devices during normal tests. If a fault is diagnosed and it is confirmed that the test needs to be discontinued, the emergency unit will replace the underwater main control unit to dispatch other controllers to complete emergency self-rescue.

Under normal working conditions, the underwater main control unit is the core of the control system of the unmanned vehicle, and it dispatches various functional units to realize information sharing and coordinated operation. As shown in Fig. 2, information transmission and work flow of the control system of the unmanned vehicle can be divided into five steps (①–⑤). Step ① indicates that the underwater main control unit inquires the basic control unit, the power unit, and the navigation unit to obtain real-time rudder angles, rotational speeds, and pose from navigation sensors. Step ② shows that the underwater main control unit sends the information inquired in Step ① to the motion planning and control unit. In Step ③, the motion planning and control unit solves speed and rudder-angle instructions based on real-time data of the unmanned vehicle and sends these instructions to the underwater main control unit. Step ④ demonstrates that the underwater main control unit sends the received rudder-angle and speed instructions to the basic control unit and the power unit, respectively. Step ⑤ indicates that the underwater main control unit sends the state of the unmanned vehicle to the emergency unit for fault diagnosis and to the underwater storage unit for storage.

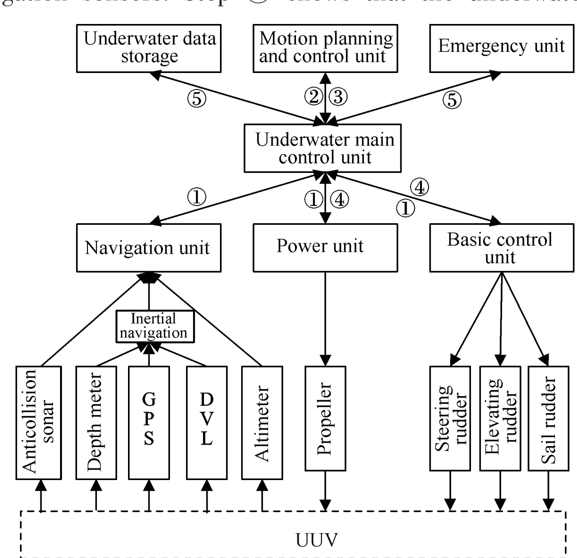

Fig.2 Structure diagram of control system for the UUV

3 Principle of navigation control

3.1 Adaptive guidance

During the path tracking of the unmanned vehicle, an adaptive guidance law based on line-of-sight (LOS) angles was introduced in this paper. This provides motion guidance in accordance with characteristics of maneuverability for the unmanned vehicle. In addition, it also provides a safe and feasible basis of motion-attitude adjustment for calculating control instructions of the vehicle in high-speed motion. For the tracking of a planned path, a virtual target point can be selected on the reference path. This target point is not strictly time-restricted and can accelerate or decelerate accordingly to cooperate with the unmanned vehicle to reduce tracking errors. The idea of providing extra degrees of freedom without the direct influence of time makes the path-tracking system more robust, and ensures a smooth trajectory of the unmanned vehicle at a high speed. Moreover, it can resist interference from external environment without destabilizing the closed-loop control system.

Suppose that the unmanned vehicle is approaching a curved path (Fig. 3), and that there is a virtual target point P on the curved path at the current moment. A Serret-Frenet coordinate system $\{F\}$ is defined along the tangent direction with respect to the curved path at the target point and according to the right-hand rule. Then, equations of path-tracking errors of the unmanned vehicle in the Serret-Frenet coordinate system are established as follows [9]:

$$\begin{cases} x_{\mathrm{e}} = \cos(\psi_P)\cos(\theta_P)(x-x_P)+\sin(\psi_P)\cos(\theta_P)(y-y_P)- \\ \sin(\theta_P)(z-z_P) \\ y_{\mathrm{e}} = -\sin(\psi_P)(x-x_P)+\cos(\psi_P)(y-y_P) \\ z_{\mathrm{e}} = \cos(\psi_P)\cos(\theta_P)(x-x_P)+\sin(\psi_P)\sin(\theta_P)(y-y_P)+ \\ \cos(\theta_P)(z-z_P) \end{cases} \tag{1}$$

where $\psi_P = \mathrm{atan2}(\dot{y}_P, \dot{x}_P)$; " · " means derivation; $\theta_P = \arctan\left(-\dot{z}_P / \sqrt{\dot{x}_P^2 + \dot{y}_P^2}\right)$; (x, y, z) and (x_P, y_P, z_P) are coordinates of the unmanned vehicle and the virtual target point in a geodetic coordinate system $\{E\}$, respectively; (x_e, y_e, z_e) are position errors between the unmanned vehicle and the virtual target point in the Serret–Frenet coordinate system. In Fig. 3, $\{B\}$ is a vehicle–body coordinate system; U_B is a direction of motion; $\{E\}$ is the geodetic coordinate system; R is a reference point; x_b, y_b and z_b are axes of the coordinate system $\{B\}$; ξ, ζ and η are axes of the coordinate system $\{E\}$; β and α are a drift angle and an attack angle of the unmanned vehicle, respectively; ψ_{LOS} is a heading guidance angle; θ_{LOS} is a depth guidance angle.

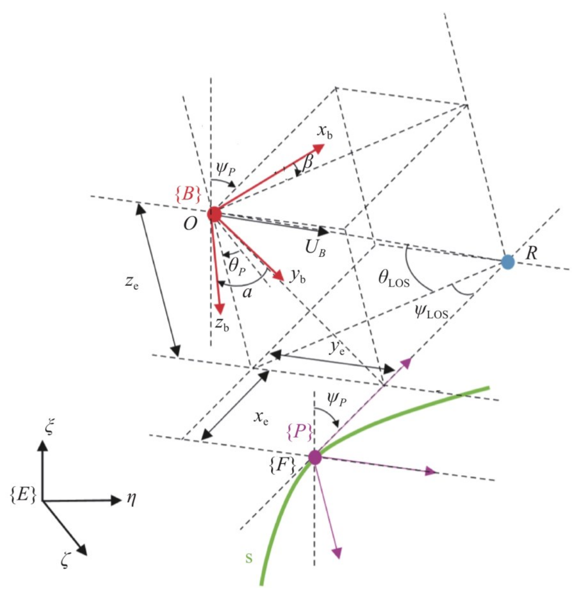

Fig.3 Diagram of path following in 3D space

According to the position errors given by Eq. (1), the path–tracking guidance law is designed as shown in Eq. (2).

$$\begin{cases} \psi_{\mathrm{LOS}} = \arctan\left(\dfrac{-k_y y_e}{\Delta y}\right) \\ \theta_{\mathrm{LOS}} = \arctan\left(\dfrac{k_z z_e}{\Delta z}\right) \end{cases} \tag{2}$$

where Δy and Δz are LOS distances; k_y and k_z are guidance gains. k_y, Δy, k_z and Δz are positive real numbers. Usually, Δy and Δz are set to twice the length of the unmanned vehicle. Intelligent steering behavior similar to that of a steersman in operating a rudder is obtained by changing the speed of the unmanned vehicle approaching a target path through adjustment of k_y and k_z. Obviously, an experienced steersman will change steering behavior according to variations of a heading target. If the target trajectory approaches a steeper curve, the steersman will increase the steering angle in advance, so that the vehicle can still adapt to the changing direction of the trajectory to automatically change the course in high–speed navigation. If a straight line is followed as required, the steersman will gradually reduce the steering angle to make the vehicle trajectory gradually approach a straight line. Therefore, gains of LOS guidance can be changed adaptively by planning curvature characteristics of trajectories to improve the control performance of vehicles at high speeds.

ψ_{LOS} and θ_{LOS} in Eq. (2) are obtained in the Serret– Frenet coordinate system. However, actual control needs to be completed in the geodetic coordinate system $\{E\}$. Therefore, it is necessary to convert ψ_{LOS} and θ_{LOS} into the geodetic coordinate system, and the converted ψ_{d} and θ_{d} can be calculated by Eq. (3).

$$\begin{cases} \theta_{\mathrm{d}} = \arcsin[\sin(\theta_P)\cos(\theta_{\mathrm{LOS}})\cos(\psi_{\mathrm{LOS}}) + \\ \cos(\theta_P)\sin(\theta_{\mathrm{LOS}})] \\ \psi_{\mathrm{d}} = \mathrm{atan2}[\cos(\psi_P)\sin(\psi_{\mathrm{LOS}})\cos(\theta_{\mathrm{LOS}}) - \\ \sin(\theta_P)\sin(\theta_{\mathrm{LOS}})\sin(\psi_P) + \\ \sin(\psi_P)\sin(\psi_{\mathrm{LOS}})\cos(\theta_P)\sin(\theta_{\mathrm{LOS}}) - \\ \sin(\psi_P)\sin(\psi_{\mathrm{LOS}})\cos(\theta_{\mathrm{LOS}}) - \\ \sin(\theta_P)\sin(\theta_{\mathrm{LOS}})\sin(\psi_P) + \\ \sin(\psi_P)\cos(\psi_{\mathrm{LOS}})\sin(\theta_P)\cos(\theta_{\mathrm{LOS}})] \end{cases} \tag{3}$$

In practical application, ψ_{d} and θ_{d} can be simplified. According to spatial projection relations[10], ψ_{d} and θ_{d} are simplified as follows.

$$\begin{cases} \psi_{\mathrm{d}} = \psi_{\mathrm{LOS}} + \psi_P - \beta \\ \theta_{\mathrm{d}} = \theta_{\mathrm{LOS}} - \theta_P + \alpha \end{cases} \tag{4}$$

To guide the unmanned vehicle to approach a target path (the target path is a parameterized curve with respect to an independent variable ω), the virtual target point needs to synergistically accelerate or decelerate. To obtain the update rate $\dot{s}$ of the virtual target point, the moving speed U_P of the virtual target point is designed as follows:

$$U_P = U_{\mathrm{d}}\cos(\psi_{\mathrm{LOS}})\cos(\theta_{\mathrm{LOS}}) + k_x x_e \tag{5}$$

where U_{d} is the expected speed of the unmanned vehicle at the current time; k_x is the gain, which is a positive real number. Then, $\dot{\omega}$ can be obtained as follows:

$$\dot{\omega} = \frac{U_P}{\sqrt{(\mathrm{d}x_P/\mathrm{d}\omega)^2 + (\mathrm{d}y_P/\mathrm{d}\omega)^2 + (\mathrm{d}z_P/\mathrm{d}\omega)^2}} \tag{6}$$

To verify effectiveness of the above guidance law, a Lyapunov function V is defined as follows.

$$V = \frac{1}{2}\boldsymbol{\varepsilon}^{\mathrm{T}}\boldsymbol{\varepsilon} \tag{7}$$

where $\boldsymbol{\varepsilon} = [x_e, y_e, z_e]^{\mathrm{T}}$. Taking derivatives of V, we can obtain

$$\dot{V} = x_e\left[U_d\cos\left(\psi_{LOS}\right)\cos\left(\theta_{LOS}\right) - U_P\right] + y_e U_d\sin\left(\psi_{LOS}\right)\cos\left(\theta_{LOS}\right) - z_e U_d\sin\left(\theta_{LOS}\right) \tag{8}$$

Substituting Eq. (5) into Eq. (8), we can get

$$\dot{V} = -k_x x_e^2 + y_e U_d\sin\left(\psi_{LOS}\right)\cos\left(\theta_{LOS}\right) - z_e U_d\sin\left(\theta_{LOS}\right) \tag{9}$$

Substituting Eq. (2) into Eq. (9), we can obtain

$$\dot{V} = -k_x x_e^2 - U_d\left[\cos\left(\theta_{LOS}\right)\frac{k_y y_e^2}{\sqrt{\left(k_y y_e\right)^2 + \Delta y^2}} + \frac{k_z z_e^2}{\sqrt{(k_z z_e)^2 + \Delta z^2}}\right] < 0 \tag{10}$$

Thus, it can be proved that path-tracking errors will converge to zero under the designed guidance law.

The large-scale high-speed UUV in this paper has a large test-speed range of 6–17 kn. Therefore, to ensure path-tracking capacity of the unmanned vehicle at each speed, guidance gains are adjusted in a fuzzy manner to realize adaptive guidance in 3D space. The designed adaptive guidance gain is as follows.

$$k_* = k_{*\min} + w_*(k_{*\max} - k_{*\min}) \tag{11}$$

where * represents y or z; $k_{*\min}$ and $k_{*\max}$ are minimum and maximum guidance gains, respectively; w_* is the regulation factor determined by a fuzzy controller, and $w_* \in [0,1]$. Then, input E_* of the fuzzy controller is defined as follows:

$$\begin{cases} E_* = \mathrm{abs}(*_e) \\ \dot{E}_* = \mathrm{d}E_*/\mathrm{d}t \\ w_* = f_*(E_*, \dot{E}_*) \end{cases} \tag{12}$$

In Eq. (12), f_* is the corresponding fuzzy controller. f_* defines five fuzzy subsets {*NB*, *NS*, *Z*, *PS*, *PB*} (*NB*: negatively big, *NS*: negatively small, *Z*: zero, *PS*: positively small, and PB: positively big). Normalized input is determined by a triangular membership function, and Mamdani reasoning is carried out according to the fuzzy rules given in Table 1. Finally, results of the center-of-gravity method are used as regulation factors of guidance gains after fuzzy adjustment.

Table 1 Fuzzy control rules utilized for adaptive guidance law

$E_*/w_*/\dot{E}_*$	*NB*	*NS*	*Z*	*PS*	*PB*
NB	*PS*	*PS*	*Z*	*NS*	*NB*
NS	*PS*	*Z*	*NS*	*NS*	*NB*
Z	*Z*	*NS*	*NS*	*NB*	*NB*
PS	*N*	*NS*	*NS*	*NB*	*NB*
PB	*NS*	*NS*	*NB*	*NB*	*NB*

3.2 Motion control

According to practical engineering experience, for a slender vehicle with symmetrical port and starboard sides and a great aspect ratio, its motion can be decomposed in terms of longitudinal and transverse motion. Specifically, forward speed control can be further decoupled from the longitudinal subsystem for separate control. Therefore, by using the method of decoupling control, this paper designed independent controllers for speed, heading, trim angles, and depth of the unmanned vehicle. This can guarantee the completion of various test actions of the unmanned vehicle, such as course keeping, course adjustment, depth keeping, depth adjustment, fixed-depth direct navigation, and path tracking, through the cooperation of various controllers.

A PID controller is a widely used, simple, and practical controller. An integral element in the PID controller can eliminate static errors and improve control accuracy. However, in the case of process initiation and termination, or great increase and decrease in setting values, it will cause integral accumulation, thus bringing about system overshoot or oscillation. For a high-speed vehicle, the system overshoot and oscillation will increase the risk of navigation out of control. Therefore, based on a traditional PID controller, this paper introduced the idea of integral separation to eliminate the above adverse effects while improving static response characteristics of the high-speed large-scale unmanned vehicle. Let the proportional coefficient, integral coefficient, and differential coefficient of a digital PID controller be κ_p, κ_i, and κ_d, respectively. Then, the discrete expression of output of the k-th step is as follows.

$$u(k) = \kappa_p e(k) + \kappa_i\sum_{j=0}^{k} e(k) + \kappa_d\frac{e(k) - e(k-1)}{T} \tag{13}$$

where $e(k)$ is the k-th error; T is a period, s.

In combination with the idea of integral separation:

1) An error threshold σ is set;

2) In the case of $|e(k)| > \sigma$, PID control is applied to avoid excessive overshoot and ensure a high response speed of the system.

3) In the case of $|e(k)| \leqslant \sigma$, PID control is applied to ensure control accuracy.

This paper combined the adaptive guidance method given above and the motion-control algorithm described in this section. In addition, it introduced filters of set instructions and state feedback. Thus, a working principle diagram of the navigation control system was obtained, as shown in Fig. 4.

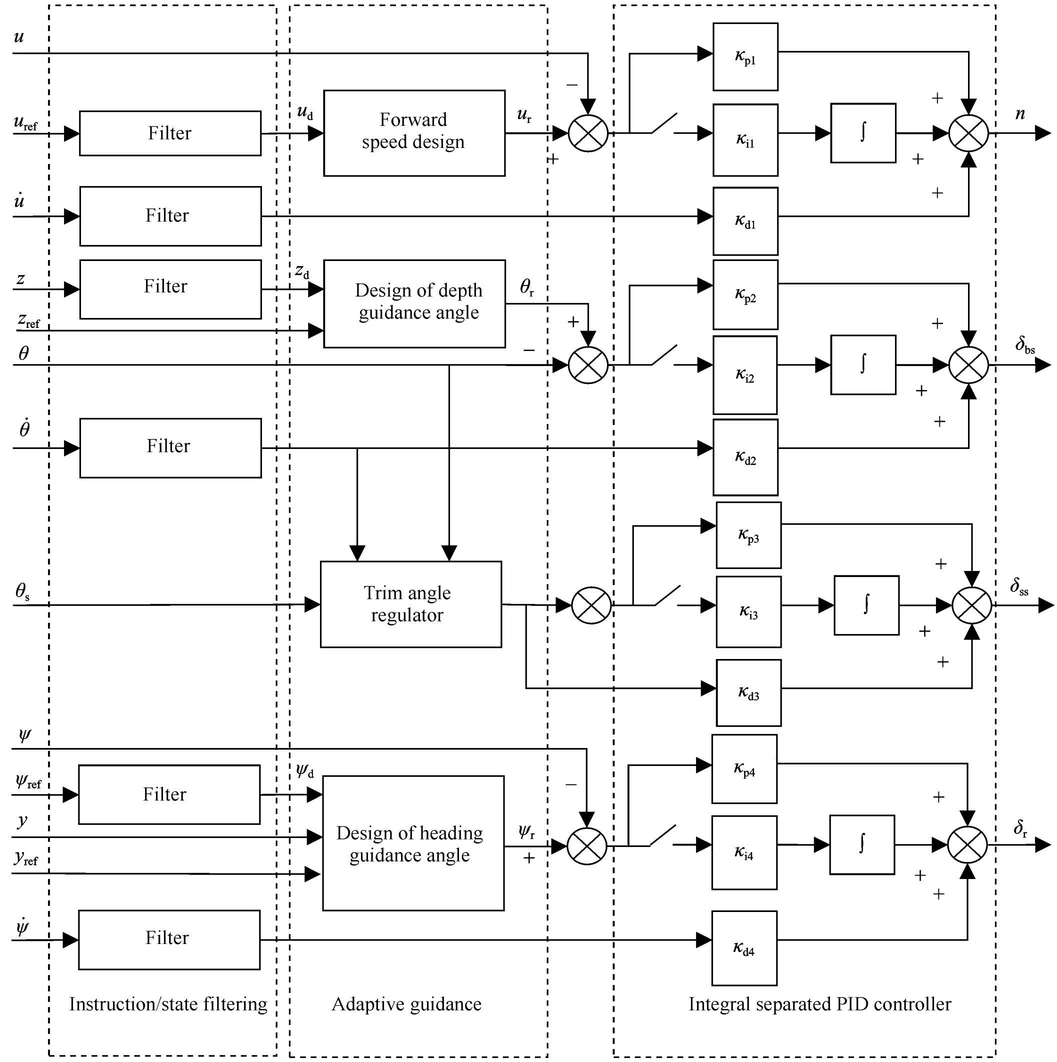

Fig.4 Diagram of dynamic control system

Table 2 lists the definitions of the variables used in Fig. 4.

Table 2 Variable definition in control algorithm

Variable	Definition	Variable	Definition
u	Forward speed	z_{ref}	Planned depth
u_{ref}	Specified speed	ψ	Heading angle
$\dot{u}$	Forward acceleration	ψ_{ref}	Planned heading angle
θ	Trim angle	$\dot{\psi}$	Heading angle velocity
$\dot{\theta}$	Change rate of trim angles	y	Horizontal ordinate
θ_s	Limited scope of trim angles	y_{ref}	Planned horizontal ordinate
u_d	Specified speed after filtering	n	Propeller speed
z_d	Planned speed after filtering	δ_{bs}	Sail rudder angle
ψ_d	Planed heading angle after filtering	δ_{ss}	Stern elevating-rudder angle
ψ_r	Heading angle of guidance	δ_r	Stern steering-rudder angle
u_r	Forward speed of guidance	z	Actual depth
θ_r	Trim angle of guidance		

The motion controller uses second-order filters to realize differential calculation of variables, and the structure of a filter is shown in Fig. 5. Specifically, x_c is the variable to be filtered; x_c^f and $\dot{x}_c^f$ are the filtered variable and its differential value; C is the damping coefficient of the filter; ω_f is natural frequency of the filter.

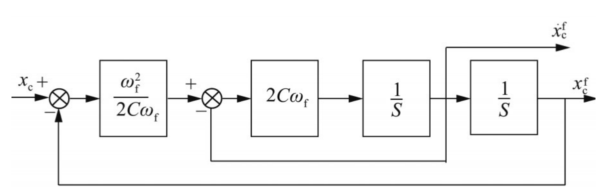

Fig. 5 Framework of second-order filter

The spatial state equations of the filter obtained from Fig. 5 are as follows.

$$\begin{cases} \dot{z}_1 = z_2 \\ \dot{z}_2 = -2C\omega_f z_2 - \omega_f^2 (z_1 - x_c) \end{cases} \tag{14}$$

where there are $z_1 = x_c^f$ and $z_2 = \dot{z}_c^f$. According to Eq. (14), if the input signal x_c is bounded, then the output signals x_c^f and $\dot{x}_c^f$ are bounded and continuous. Errors of the filter can be adjusted by ω_f. The higher the ω_f is, the faster and more accurately the output signals of the filter can follow its input ones.

The introduction of filters can obtain expected gradually varying instructions and smooth state feedback information. Moreover, the first-order differential signal $\dot{x}_c^f$ obtained by the integral method can effectively overcome disturbance of the amplified noise signals caused by differential operation on input signals. This avoids the rapid saturation, great overshoot, and even oscillation of driving actuators caused by sudden changes in instructions during high-speed motion. Thus, dynamic response characteristics of the large-scale high-speed unmanned underwater vehicle can be improved.

4 Analysis of results of lake trials

Navigation tests of the large-scale high-speed unmanned underwater vehicle were carried out in an inland reservoir, and the test water area and test channel are shown in Fig. 6. Red solid lines are channels for the unmanned vehicle to complete test motion. To reserve enough acceleration space to achieve a specified test speed, the unmanned vehicle needs to travel to and from both ends of the reservoir along two different courses. During the testing, the unmanned vehicle was first remotely controlled to be in the vicinity of the starting point of a target course. Then, the unmanned vehicle was switched to an autonomous mode. After the successful switching, the unmanned vehicle would approach the target course and dive to a test depth under the action of the navigation controller. When it was about to reach the end of the target course, the unmanned ship would automatically float up and remotely send a test completion signal, waiting for the next test task.

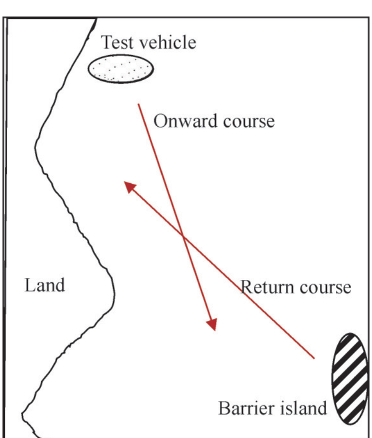

Fig. 6 Diagram of test lake and course

The large-scale high-speed UUV is a comprehensive test platform of navigation performance. Based on the navigation data obtained from a performance test of propellers, performance of the control system was analyzed in this paper. In the performance test of propellers, the unmanned vehicle was required to first dive to a specified depth and then travel steadily at a fixed speed along a fixed course for a period. During the process, it was required that attitude and rudder angle oscillations should occur as little as possible. Any form of attitude fluctuation or steering behavior during testing would affect speed and propeller noise of the unmanned vehicle. Thus, the performance test of propellers had strict requirements on navigation control capabilities of the control system.

Figs. 7-9 show the results of the fixed-depth direct-navigation tests carried out to guarantee performance tests of propellers. Actual speeds, heading angles, depths, trim angles, path-tracking results, and lateral offsets at the test speeds of 6, 9 and 13 kn are given respectively in the figures. Specifically, speed charts can show speed control capabilities of the navigation controller. Charts of heading angles, path-tracking results, and lateral offsets can show path-tracking capabilities of the navigation controller. Charts of depths and trim angles can show depth-control capabilities of the navigation controller. As can be seen from the figures, the speed control of the unmanned vehicle is stable. In terms of control of heading angles, depths, and trim angles, overshooting and small fluctuation near target values occur. In addition, during the path tracking, the unmanned vehicle moves wanders to the left and right alternately while following a target course. According to the test results, with the designed navigation control algorithm, the control system of the unmanned vehicle has the ability to adjust poses of the unmanned vehicle. It can also smoothly and stably control the unmanned vehicle to approach a target course and depth, and then complete fixed-depth direct navigation at a stable speed. Thus, it meets the requirements of the propeller performance test on the accuracy of pose control. In addition, the speed, depth, and path-tracking control are stable in the whole test section, which reflects the robustness of the navigation control algorithm. Although the performance of this control algorithm meets the test requirements, in-depth analysis of the reasons for the course and depth fluctuations should be carried out. First, limited steering frequency increases difficulty of navigation control. Second, a mechanical clearance of about 2° in steering rudder gears affects course control, and residual buoyancy of the unmanned vehicle affects depth control. The above factors lead to fluctuations of heading angles and depths of the unmanned vehicle during its navigation. However, the control system has reduced effects of the above unfavorable factors on accuracy of pose control to a reasonable degree as far as possible.

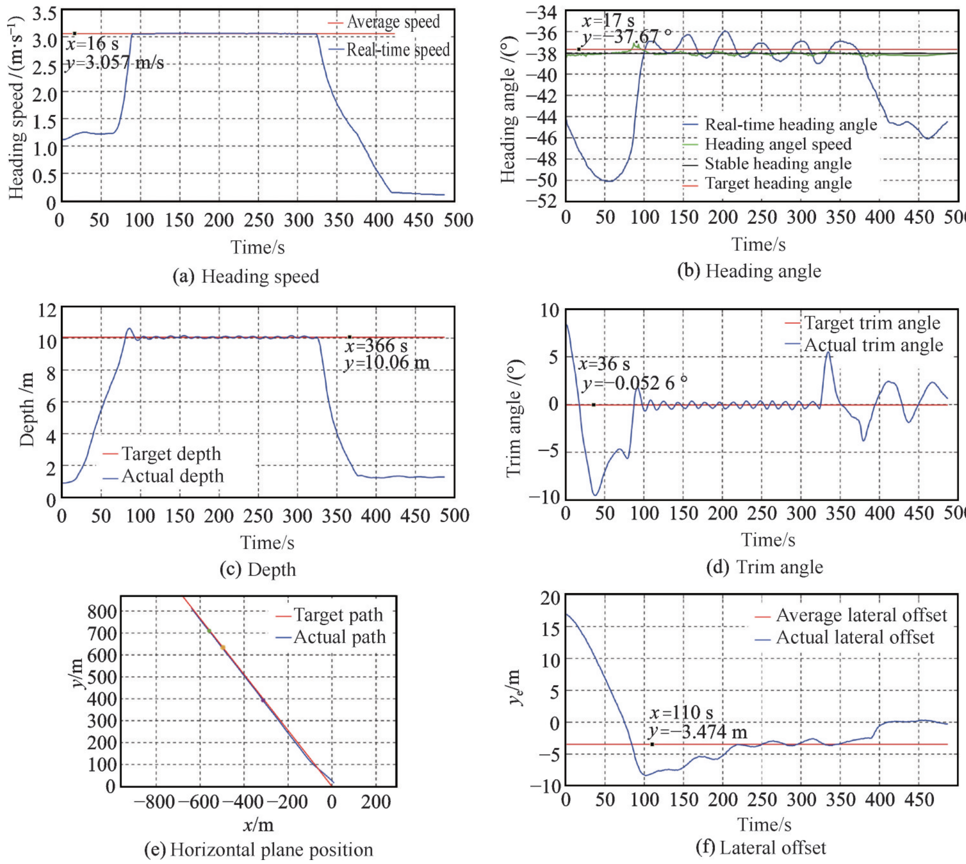

Fig.7 Test results of depth keeping in direct navigation at 6 kn

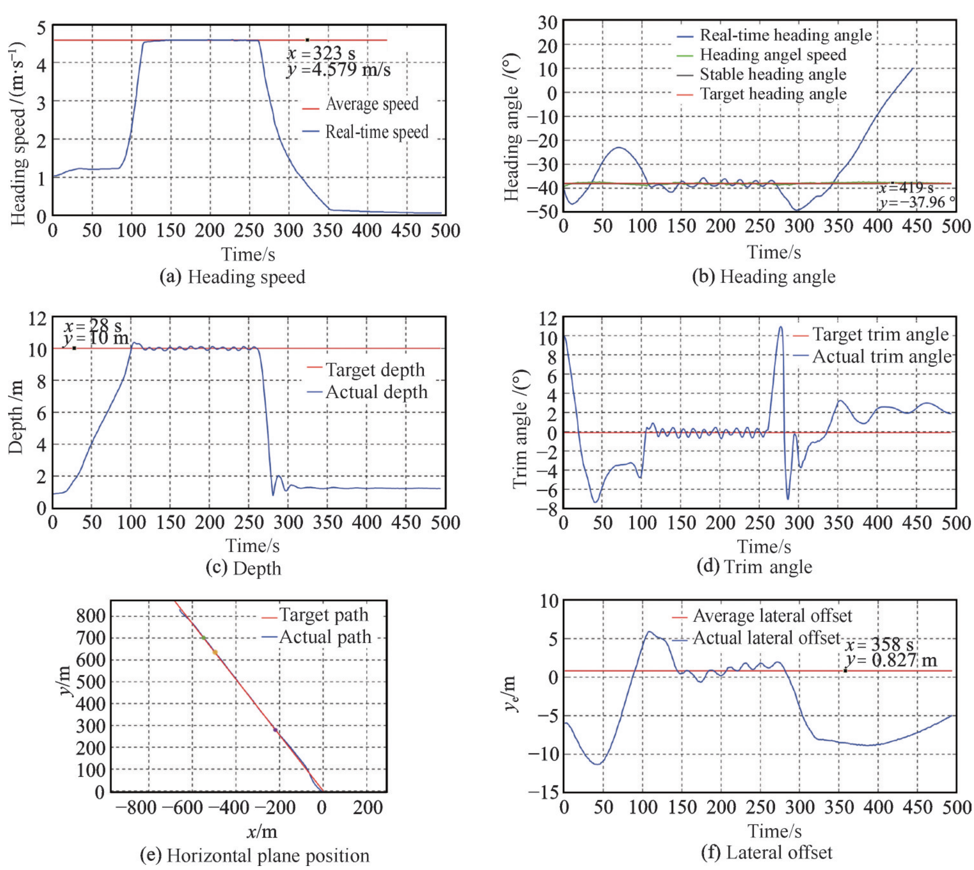

Fig.8 Test results of depth keeping in direct navigation at 9 kn

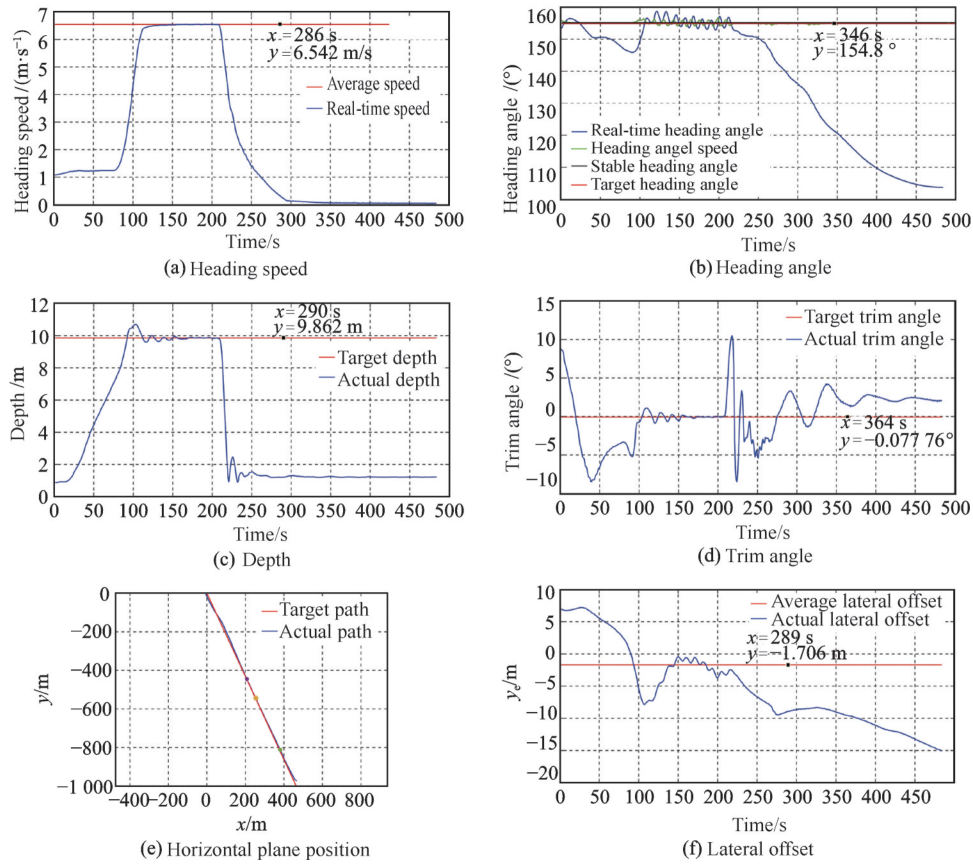

Fig.9 Test results of depth keeping in direct navigation at 13 kn

Table 3 shows the quantitative analysis results of the tests. According to the table, the large-scale high-speed UUV has a course-control deviation of less than 2° and a depth-control deviation of less than 0.2 m. Thus, the control results are good enough to meet technical requirements related to propeller performance tests.

Table 3 Analysis results of navigation test

Parameter	Speed/kn		
	6	9	13
Stable speed /($m \cdot s^{-1}$)	3.057	4.579	6.542
Heading deviation range/(°)	−1.3~1.7	−1.5~2.2	−2.0~2.3
Stable heading angle/(°)	−37.6	−37.9	154.8
Depth fluctuation range/m	9.96~10.16	9.87~10.13	9.79~9.97
Stable depth /m	10.06	10	9.862
Trim deviation range/(°)	−0.54~0.39	−0.75~0.47	−0.58~0.17
Stable trim angle /(°)	−0.05	−0.09	−0.07
Offset fluctuation range/m	−1.78~0.87	−1.48~1.04	−2.03~1.26
Stable offset/m	−3.47	0.82	−1.7

5 Conclusions

The large-scale high-speed UUV described in this paper is a special unmanned underwater vehicle for testing maneuverability, rapidity, and invisibility of submarines. On the basis of analyzing such hardware configurations as actuators and sensors of the unmanned vehicle, this paper proposed a framework for the control system of the unmanned vehicle. The control system takes an underwater main control unit as the core. In addition, it is equipped with a navigation unit, a motion planning and control unit, a power unit, a basic control unit, an emergency unit, and an underwater data storage unit, according to functions. In order to meet the task requirements of the unmanned vehicle as a comprehensive test platform, this paper designed a fuzzy adaptive guidance method to ensure that the unmanned vehicle can smoothly complete 3D path tracking at all test speeds. Considering the characteristics of large inertia and high speed of the unmanned vehicle, this paper designed PID controllers for speed, heading, depth, and trim angle control respectively based on the idea of integral separation. The introduction of instruction and state filters avoids the output saturation, large overshoot, and even oscillation caused by sudden changes in instructions in high-speed motion. Thus, this improves dynamic response characteristics of the unmanned vehicle. According to the lake trial results, the navigation control algorithm is able to control the poses of the unmanned vehicle, with stable performance and robustness. Therefore, it has certain reference significance for studying motion control technologies of new-generation unmanned test vehicles.

References

[1] PFITSCH D, GORDON B, RICE J, et al. Development and deployment of autonomous scale submarine models for hydrodynamic testing of U.S. Navy submarine maneuvering characteristics[C]. //Proceedings of OCEANS 2016 MTS/IEEE. Monterey: IEEE, 2016: 1-6.

[2] CHASE N, MICHAEL T, CARRICA P M. Overset simulation of a submarine and propeller in towed, self-propelled and maneuvering conditions [J]. International Shipbuilding Progress, 2013, 60 (1/2/3/4): 171-205.

[3] WEI J, CHEN Z C, ZENG B. Design of submarine self-propelled model control system [J]. Fire Control & Command Control, 2014, 39 (11): 171-174 (in Chinese).

[4] YANG J J, LI W J. Reliability optimization design of submarine free-running model systems [J]. International Journal of Engineering and Technology, 2016, 8 (5): 323 - 328.

[5] CHEN D B. Design and composition of a self-propelled model test system for manoeuvrability of submarines [J]. Ship & Boat, 2012, 23 (6): 22 - 26 (in Chinese).

[6] HUMPHREYS D E, WATKINSON K W, CARAMANICA P. Use of the navy's large scale vehicle kokanee (LSV 1)to investigate near-surface effects on maneuvering characteristics [C]. //Proceedings of International Symposium on Unmanned Untethered Submersible Technology. Durham, NH: University of New Hampshire, 1999: 203-210.

[7] CARPENTER B, RICHARDSON M, et al. Large scale vehicle 2 (LSV2) aval research platform [D]. Moscow: University of Idaho, 2009.

[8] LIU Y, XIAO C R, DU P P. Design of the self-propelled model for submarine maneuvering ability tests [J]. Ship & Ocean Engineering, 2016, 45 (1): 6-12 (in Chinese).

[9] XIANG X B, YU C Y, ZHANG Q. Robust fuzzy 3D path following for autonomous underwater vehicle subject to uncertainties [J]. Computers & Operations Research, 2017, 84: 165-177.

[10] WANG G X, XU G H, LIU G, et al. Fuzzy iterative sliding mode control applied for path following of an autonomous underwater vehicle with large inertia [J]. Mathematical Problems in Engineering, 2019 (1): 1-14.

大尺度高速水下无人艇控制系统设计与试验验证

王文晋, 王冠学, 李奔, 徐国华*

华中科技大学 船舶与海洋工程学院, 湖北 武汉 430074

摘　要:[**目的**]为了在三维空间宽航速段内实现大尺度高速水下无人艇(UUV)的路径跟踪,在考虑无人艇的试验动作要求、控制精度要求及水动力特性的情况下,设计了基于模糊控制理论的自适应制导方法。[**方法**]基于解耦控制方法,首先将水下无人艇的航行控制分解为航速、航向、纵倾和深度控制问题;然后分别设计积分分离比例—积分—微分控制器(PID 控制器),并引入指令及状态滤波器,以改善该水下无人艇动态响应特性;最后,通过湖试验证水下无人艇在不同航速下的控制性能。[**结果**]结果表明,在6,9,13 kn 等试验航速下,水下无人艇跟随目标路径和深度的误差均在合理范围内,验证了该控制体系及控制方法的有效性。[**结论**]所得结果对新一代试验艇的运动控制技术研究具有一定参考价值。

关键词: 无人水下航行器; 试验艇; 自适应制导; 积分分离 PID; 二阶滤波器